IEEE Access
Multidisciplinary | Rapid Review | Open Access Journal

Received February 25, 2019, accepted March 12, 2019, date of publication March 29, 2019, date of current version April 13, 2019.

Digital Object Identifier 10.1109/ACCESS.2019.2907176

Harmonic Quantitative Analysis for Dead-Time Effects in SPWM Inverters

NING JIAO[1], SHUNLIANG WANG[1], (Member, IEEE), TIANQI LIU[1], (Senior Member, IEEE), YANBO WANG[2], (Member, IEEE), AND ZHE CHEN[2], (Fellow, IEEE)

[1]College of Electrical Engineering and Information Technology, Sichuan University, Chengdu 610065, China
[2]Department of Energy Technology, Aalborg University, 9220 Aalborg, Denmark

Corresponding author: Shunliang Wang (slw_scu@163.com)

This work is supported in part by the National Natural Science Foundation of China under Grant 51707126 and in part by the Fundamental Research Funds for the Central Universities under Grant 2017SCU12013.

ABSTRACT Dead-time is commonly designed to avoid shoot-through phenomenon within each arm in voltage source converter. The presence of dead-time tends to cause a power quality issue. Quantitative analysis for dead-time effects is important to mitigate power quality issue. This paper presents two harmonic quantitative analysis methods for dead-time effects in SPWM inverters. First, the harmonic analysis method based on double Fourier series is modified to adapt any initial phase angle and calculate additional harmonics from dead-time effects. Then, a calculation method for switching angles in sinusoidal pulse width modulation (SPWM) is presented. Based on the obtained switching angles and single Fourier series, a more concise calculation method is proposed to perform quantitative analysis for the impact of dead-time on harmonics. The harmonic model is able to reveal the mechanism of harmonics generation from dead-time. Finally, the inner relationship and essential difference between double- and single-Fourier series are summarized. The simulation and experimental results show that both of the proposed quantitative analysis methods can accurately evaluate the effect of dead-time on harmonics.

INDEX TERMS Harmonics, dead-time, double Fourier series, single Fourier series, SPWM.

I. INTRODUCTION

As the increasing penetration of renewable energies-based distributed generation (DG) systems, power electronic converters are becoming an important interface to integrate renewable energies into utility grid. However, several technical challenges become apparent and one of which is pertaining to the impact of the power quality [1]–[2]. In voltage source converter (VSC), pulse width modulation (PWM) strategies have been widely applied to enable switching control of power devices [3]–[4]. To make assure safe operation, dead-time is always designed to avoid simultaneous conduction of power devices within up-arm and down-arm. However, the presence of dead-time tends to cause current distortion and voltage harmonics, which thus degrades operation performance of VSC [5]–[6]. Also, the distorted current and voltage harmonics can cause further side-effects on the power grid [7]–[8], such as harmonic instability [9]–[10] or harmonic resonance [11]–[12]. Accurate evaluation of harmonic content can contribute to harmonic suppression. Therefore, it is significant to develop quantitative analysis method to evaluate influences of dead-time effects on harmonic performance of VSC.

Previous work in [13]–[14] have been presented to analyze harmonics mechanism caused by PWM. Analysis methods of harmonic characteristic mainly include double Fourier series [4], [14]–[19] and single Fourier series [20]–[23].

The double Fourier series is a method originally developed by Bennett and Black and later adopted for a PWM switching waveform by Bowes and Bird [13]. This method is able to derive harmonic distribution characteristics, but it is challenging to understand and apply. A method based on double Fourier series is presented to calculate harmonic spectrum in two-level PWM converter [14]–[15] and multilevel PWM converter [4], [16]. But it did not consider the impact of dead-time effects. The analysis of dead-time effects applying 3-D geometric wall contour models is performed in [17], where the harmonic voltage models are presented with the double Fourier series approach. However, the analysis procedure is complicated as there are two reference angles that based on carrier wave and modulation wave respectively needed to be considered, and Bessel functions are used.

The associate editor coordinating the review of this manuscript and approving it for publication was Poki Chen.

Reference [18] analyzes the output harmonics of an H-Bridge Inverter with dead-time from two parts: an ideal part representing the PWM signal without dead-time and a correction part representing the effects caused by the dead time by applying double Fourier analysis to the 3-D mode. The method to analyze the dead-time effect in [18] can show the influence of dead-time on phase voltage more clearly, and it is clear and easy to understand. This harmonic analysis method with consideration of dead-time is also applied in [19], and the formula of harmonic with dead-time is deduced in multisampling technique. The harmonic analysis models based on double Fourier series are obtained by complicated mathematical derivation, which increases computational burdens and reduce analysis efficiency.

Another effective harmonic analysis approach is single Fourier series [20]-[23]. Reference [20] analyzes harmonics by single Fourier series, but the switching angles are represented by Kapteyn Series, which is complicated. This method is applied in [21] to analyze harmonic spectrum at a half-bridge dc/ac converter with single- and multiple-frequency modulation. In [22], the double-edge modulator be represented by two sing-edge modulators to derive expressions for the harmonic spectra of double-edge PWM waveforms in one-dimensional spectral analysis. However there is no experimental verification was performed. In [23], multilevel PWM waveform be separated into a spectral image of the reference and sideband basis functions which are then expanded using a one-dimensional Fourier series based on [22]. But the computational procedure and expression of switching angle in these aforementioned works are very complicated. They do not analyzes the impact of dead-time on harmonics and establish a harmonic model with dead-time effects based on single Fourier series, which is thus difficult to provide an applicable dead-time design guideline in industrial implementation. In addition, there is no comparison between the computation of double and single Fourier series method.

Based on the review of previous work above, it is obvious that the analysis of phase voltage harmonics of inverters has developed from the more complex double Fourier method to the single Fourier method which is much simpler, and the effect of phase voltage harmonics with dead-time effects has been taken into account gradually. However, there are no in-depth study of the inner link and different between the two methods and their respective applicable scenarios.

Therefore, this paper presents a quantitative analysis method to establish compact and low computational harmonic analysis model with consideration of dead-time effects, which is able to reveal root cause of harmonic distortion caused by dead-time effects. Furthermore, the inner link and different between the two popular harmonics analysis methods, double Fourier series and single Fourier series, need to be revealed.

The rest of this paper is organized as follows. Basis of sinusoidal PWM (SPWM) and dead-time effects are introduced in Section II. In Section III, The quantitative analysis methods of harmonics and the mechanisms of harmonics generation caused by dead-time effects are proposed by double Fourier series and single Fourier series, respectively. The inner link and essential difference between the two methods are summarized by comparing the two methods. In Section IV, simulation and experimental results are given to validate the proposed harmonic analysis methods. Main conclusions are drawn in Section VII.

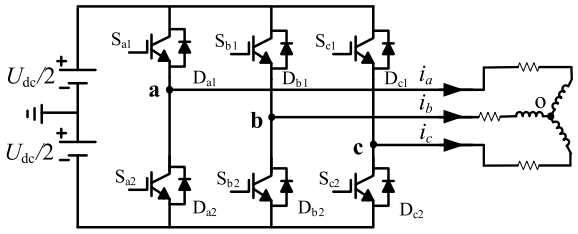

FIGURE 1. The circuit diagram of a three-phase voltage source inverter.

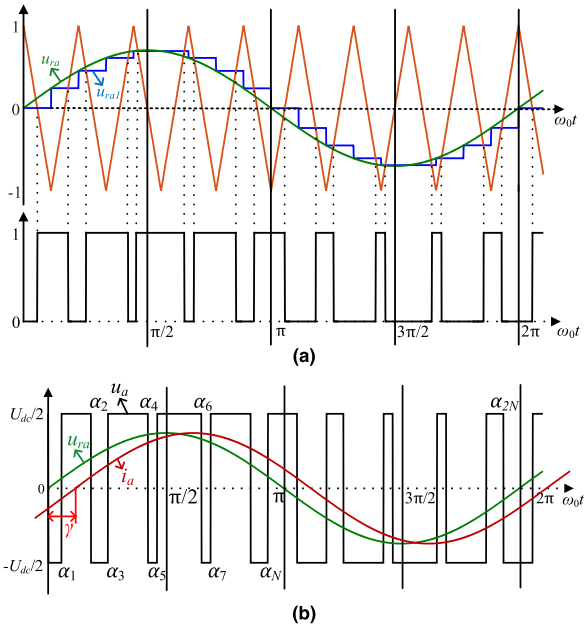

FIGURE 2. The principle of SPWM. (a) Principle of pulse generation. (b) The voltage of phase A.

II. SPWM AND DEAD-TIME EFFECTS

In this section, the basis of SPWM and dead-time effects is introduced.

A. BASIS OF SPWM

Fig.1 shows the circuit diagram of a three-phase voltage source inverter, which consists of three legs with six switching devices (S_{j1} and S_{j2} (j = a, b, c)) and six diodes (D_{j1} and D_{j2} (j = a, b, c)). U_{dc} and i_j (j = a, b, c) indicate the dc source voltage and phase current in AC side.

Compared with the symmetrical regularly sampled modulation technique, asymmetrical one that the carrier ratios is odd has the superior harmonic performance [24], which is used in this paper. Fig.2 (a) shows the principle of pulse

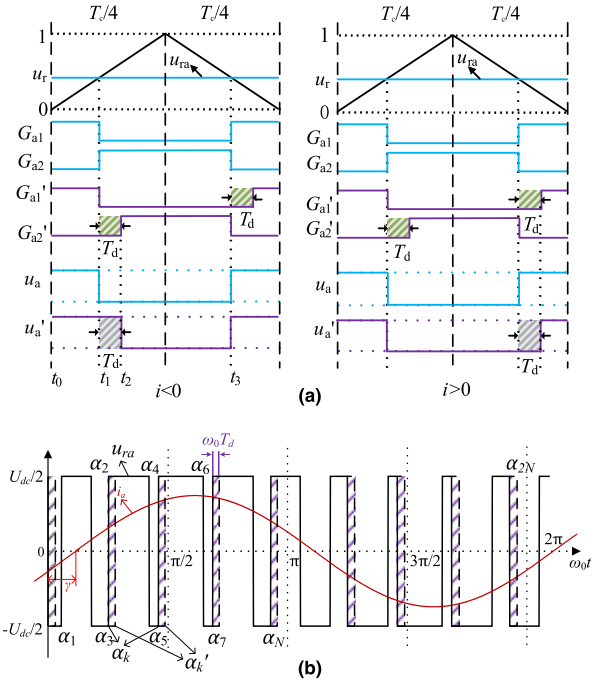

FIGURE 3. The phase A voltage with dead-time effects. (a) Dead-time effects during one switching cycle. (b) Dead-time effects during one fundamental period.

generation in SPWM strategy, where the isosceles triangle wave comparing with the modulation reference wave u_{ra} of phase **A**. If the amplitude of sinusoidal reference signal is higher than amplitude of triangle wave, the output of modulation signal is 1, otherwise it is 0.

Fig.2 (b) shows the relationship of DC-link voltage and phase **A** voltage during one fundamental period. As illustrated in Fig.2 (b), α_k is the k-th switching angle, and N is the total number of switching angles in a half of fundamental period. $N = f_c/f_0$ is carrier ratio, where f_c is the frequency of the triangular carrier signal, and f_0 is the fundamental frequency.

B. DEAD-TIME EFFECTS

Fig.3 shows principle of dead-time effects for phase **A** voltage, where G_{a1} and G_{a2} are ideal switching signals driven by PWM without dead-time effects, and G_{a1}' and G_{a2}' are switching states with consideration of dead-time effects. u_a and u_a' represent phase **A** voltage without and with dead-time. u_{ra} represents the modulation reference signal of phase **A**.

It can be seen from Fig.3 (a) that the voltage u_a and switching states are affected by dead-time effects during one switching cycle. The case about phase current $i_a < 0$ is explained as following. During the period t_0 to t_1, the phase current flow through the diode D_{a1}, and $u_a = U_{dc}/2$, as the upper switching device S_{a1} is under switching-on state and the lower switching device S_{a2} is under switching-off state. At the time instant t_1, S_{a1} is under switching-off state due to the effect of dead-time T_d. Switching S_{a1} and S_{a2} are both under switching-off state during t_1 to t_2. Therefore, the phase current flow through the diode D_{a1}, and $u_a = U_{dc}/2$ during that time because of inductor current freewheels. At the time instant t_2, S_{a2} is under turning-on state, and $u_a = -U_{dc}/2$. S_{a1} is under switching-off state During t_2 to t_3, the analysis can be performed in the same way. To sum up, if $i_a < 0$, the commutation moments of phase voltage u_a turning from $-U_{dc}/2$ to $U_{dc}/2$, and turning from $U_{dc}/2$ to $-U_{dc}/2$ are determined by the switching device S_{a2}. Similarly, if $i_a > 0$, the commutation moments of phase voltage u_a are determined by the switching device S_{a1}. Therefore, the impact of dead-time effects on outputs phase voltage is related to the direction of the output current.

Fig.3 (b) shows the modulation process influenced by dead-time effects during one fundamental period. It can be seen that the time instant of switching angels is changed due to the presence of dead-time, which thus may change harmonic characteristics.

III. HARMONIC QUANTITATIVE ANALYSIS

A. DOUBLE FOURIER SERIES

In this subsection, the double Fourier series method is introduced and modified to adapt any initial phase angle in SPWM harmonics analysis. Model of the harmonic voltage with and without dead-time effects are established in closed-form expression, respectively.

Classical double Fourier series can be expressed as

$$\begin{aligned} f(t) &= \frac{A_{00}}{2} + \sum_{p=1}^{\infty}[A_{0p}\cos p(\omega_0 t+\theta_0) + B_{0p}\sin p(\omega_0 t+\theta_0)] \\ &\quad + \sum_{q=1}^{\infty}[A_{q0}\cos q(\omega_c t+\theta_c) + B_{q0}\sin q(\omega_c t+\theta_c)] \\ &\quad + \sum_{q=1}^{\infty}\sum_{\substack{p=-\infty \\ (p\neq 0)}}^{\infty}\begin{Bmatrix} A_{qp}\cos[q(\omega_c t+\theta_c)+p(\omega_0 t+\theta_0)] \\ +B_{qp}\sin[q(\omega_c t+\theta_c)+p(\omega_0 t+\theta_0)] \end{Bmatrix} \end{aligned} \tag{1}$$

$$\begin{aligned} A_{qp} &= \frac{1}{2\pi^2}\int_{-\pi}^{\pi}\int_{-\pi}^{\pi} f(\omega_c t+\theta_c, \omega_0 t+\theta_0)\cos[q(\omega_c t+\theta_c) \\ &\quad + p(\omega_0 t+\theta_0)]d(\omega_c t+\theta_c)d(\omega_0 t+\theta_0) \\ B_{qp} &= \frac{1}{2\pi^2}\int_{-\pi}^{\pi}\int_{-\pi}^{\pi} f(\omega_c t+\theta_c, \omega_0 t+\theta_0)\cos[q(\omega_c t+\theta_c) \\ &\quad + p(\omega_0 t+\theta_0)]d(\omega_c t+\theta_c)d(\omega_0 t+\theta_0) \end{aligned}$$

where the two variable are $\omega_c t + \theta_c$ and $\omega_0 t + \theta_0$, ω_c is angular frequency of triangular carrier, θ_c is phase shift angle of triangular carrier, ω_0 is fundamental angular frequency, and θ_0 is fundamental phase offset angle. q is carrier index variable, and p is baseband index variable.

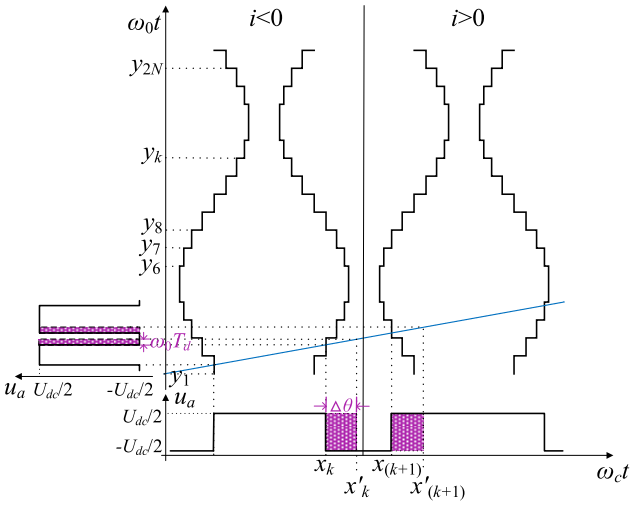

FIGURE 4. Effect of dead-time on switching angle x_k.

Setting $x = \omega_c t$, $y = \omega_0 t$. Then the coefficients A_{qp} and B_{qp} can be expressed as plural form as follows.

$$C_{qp} = A_{qp} + jB_{qp} = \frac{1}{2\pi^2}\int_{-\pi}^{\pi}\int_{-\pi}^{\pi} f(x,y)e^{j(qx+py)}dxdy \quad (2)$$

So the harmonic amplitude can be obtained as (3)

$$|C_{qp}| = \sqrt{A_{qp}^2 + B_{qp}^2} \quad (3)$$

For asymmetrical regular sampling, there are the two sampling points established in each carrier interval. The modulation wave angle y_k corresponding to the sampling time instant (in Fig.4) can be expressed as

$$y_k = \frac{\omega_0}{\omega_c}\pi(k-1) \quad k = 1, 2, 3, \cdots, 2N \quad (4)$$

Using continuous variables x and y, y_k can be expressed as

$$y_k = y - \frac{\omega_0}{\omega_c}[x - \pi(k-1)] \quad (5)$$

Defining function $g(\varphi)$ as

$$g(\varphi) = \begin{cases} -1 & \varphi \text{ corresponding the rising edge} \\ 1 & \varphi \text{ corresponding the falling edge} \end{cases} \quad (6)$$

where φ is switching angle at any position.

Different from switching angle α_k, which is reference to angle of the modulation wave, x_k is switching angle that based on the angle of the carrier as shown in Fig.4. And it can be expressed as

$$\begin{aligned} x_k &= \frac{\pi}{2} + \pi(k-1) + g(x_k)\Delta x_k \\ x_k &= \frac{\pi}{2}M\sin y_k \end{aligned} \quad (7)$$

where M is the modulation index.

The proposed solution in (7) for switching angle does not require a specific initial condition, such as zero reference angle and sampling point [17]-[24].

The harmonic coefficient in (2) can be expressed as

$$C_{qp} = \frac{U_{dc}g(x_k)}{4\pi^2}\Big(\int_0^{2\pi}\int_0^{x_k} e^{j(qx+py)}dxdy - \int_0^{2\pi}\int_{x_k}^{x_{(k+1)}} e^{j(qx+py)}dxdy + \int_0^{2\pi}\int_{x_{(k+1)}}^{2\pi} e^{j(qx+py)}dxdy\Big) \quad (8)$$

The output phase voltage is mirror symmetry due to the modulation method used in this paper. Therefore, (8) can be simplified as

$$C_{qp} = \frac{U_{dc}}{2js\pi}\frac{\omega_0}{\omega_c}\left[1-(-1)^{(Nq+p)}\right]e^{-js\frac{\pi}{2}} \times \sum_{k=1}^{N} g(x_k)e^{jks\pi}e^{g(x_k)js\frac{\pi}{2}M\sin y_k} \quad (9)$$

where $s = q + p\omega_0/\omega_c = q + p/N$.

From (9), there is no even harmonics as $Nq+p$ is the harmonic order, and $Nq+p$ is odd. In addition, the distribution of harmonics are mainly the even sideband harmonic components around odd multiples of the carrier frequency, (when the carrier index variable q is odd, the baseband index variable p is even), and odd sideband harmonic components around even multiples of the carrier frequency (when the carrier index variable q is even, the baseband index variable p is odd).

As shown in Fig.3, the dead-time effects cause a time delay T_d in rising edge of u_a if phase current $i_a > 0$. Similarly, the time delay T_d happens in falling edge of u_a if $i_a < 0$. Fig.4 shows the effect of dead-time on switching angle x_k based on the angle of the carrier.

In Fig.4, $\Delta\theta$ is the time-delay based on the angle of the carrier wave.

$$\Delta\theta = \omega_c T_d \quad (10)$$

The additional harmonic component from dead-time effects can be obtained by (11).

$$\Delta C_{qp} = \frac{V_{dc}}{4\pi^2}\left[g(x_k) - \text{sign}(i)\right]\int_0^{2\pi}\int_{x_k}^{x_k^*} e^{j(qx+py)}dxdy \quad (11)$$

where sign(·) is the sign function, and sign(i) = 1 if $i \geq 0$, sign(i) = −1 if $i < 0$.

As shown in Fig.3 and Fig.4, the change of switching angle is affected by the pulse edge state and current direction. The switching angles of x_k^* with dead-time effects can be represented as (12).

$$x_k^* = x_k + \frac{1 - \text{sign}(i)g(x_k)}{2}\Delta\theta \quad (12)$$

Simplify (11), and the additional harmonic component of the dead-time ΔC_{qp} can be expressed as

$$\Delta C_{qp} = \frac{U_{dc}}{2js\pi}\frac{\omega_0}{\omega_c}\sum_{k=1}^{2N}\left[e^{js\frac{1-\text{sign}(i)g(x_k)}{2}\Delta\theta} - 1\right]g(x_k)e^{jsx_k} \quad (13)$$

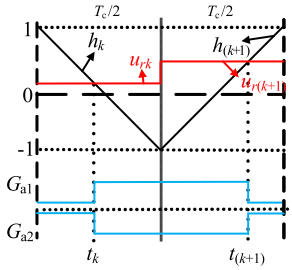

FIGURE 5. Principle of switching angles generation process.

Therefore, the harmonics of the phase voltage considering dead-time can be expressed as

$$C_{qp\text{total}} = C_{qp} + \Delta C_{qp} \tag{14}$$

B. SINGLE FOURIER SERIES

In this subsection, the computational procedure of switching angles α_k, which is reference to angle of the modulation wave, is given when asymmetrical regular sampling is applied. Then, the calculation model for harmonic analysis of SPWM based on single Fourier series is derived.

Double Fourier series analysis needs two phase spaces in carrier wave and modulation wave. That is, assuming that the voltage waveform is a periodic function of two independent variables, namely the phases of the reference and carrier waveforms. In single Fourier series analysis method, the carrier angle is converted into the angle of modulation wave, and the voltage waveform is a periodic function with only one variable, which is the phase of the reference waveform.

Fig.5 shows the principle of switching angle generation in modulation process. The original switching angle α_k ($k = 1, 2, \ldots, 2N$), which is based on modulation wave angle in a fundamental period for phase **A** voltage, can be calculated as follows. The oblique lines h_k is carrier signal of phase **A**. It can be seen from Fig.5 that the slope of oblique lines h_k is negative for t_k corresponding to the rising edge of drive signal G_{a1} and positive for t_k corresponding to the falling edge of G_{a1} in the k-th half carrier. The time instant t_k corresponding to the switching angle α_k is the intersection of the straight u_{rk} and oblique lines h_k. The straight lines u_{rk} is modulation signal for leg **A** in the k-th half carrier. ω_0 and T_c represent the angle frequency of modulation signal and triangle carrier period.

For leg **A**, the relationship between oblique lines h_k and the straight line u_{rk} are given as (15).

$$\begin{cases} h_k = g(\alpha_k)(\dfrac{4}{T_c}t - 2k + 1) \\ u_{rk} = M \sin\left[(k-1)\omega_0 \dfrac{T_c}{2}\right] = M \sin y_k \end{cases} \tag{15}$$

where t presents the time of the signal, and α_k can be obtained by the intersection of h_k and u_{rk}.

The t_k is the time instant at intersection point of oblique line h_k and straight line u_{rk}, which can be obtained from (15) as

$$t_k = \frac{T_c}{4}\left[g(\alpha_k)u_{rk} + 2k - 1\right] \tag{16}$$

So $\alpha_k (k = 1, 2, \ldots, 2N)$ in a modulation period can be given as

$$\alpha_k = \frac{\omega_0 T_c}{4}[g(\alpha_k)M \sin y_k + 2k - 1] \tag{17}$$

Combining (7) and (17), α_k can be expressed as

$$\alpha_k = \frac{\omega_0}{\omega_c} x_k \tag{18}$$

Therefore, the essence of single Fourier series analysis is to convert the carrier angle of double Fourier analysis into the angle of modulation wave and then analyze harmonics at the same reference angle.

For the phase voltage u_a in Fig.1 (c), according to Dirichlet Theorem, Fourier series of voltage u_a is given as

$$u_a = f(\omega t) = \frac{a_0}{2} + \sum_{n=0}^{\infty}(a_n \cos n\omega t + b_n \sin n\omega t) \tag{19}$$

where n is order number of spectrum; a_n and b_n are coefficients of Fourier series.

Since the output phase voltage is mirror symmetry, where the positive half-cycle waveform and the negative half-cycle waveform are symmetrical on the horizontal axis after moving the positive half-cycle waveform along the horizontal axis by half cycle. If n is even, $a_0 = a_n = b_n = 0$ can be obtained due to the symmetry. It shows that there is no dc voltage and even harmonics in the phase voltage u_a. If n is odd, the coefficients a_n and b_n can be derived as (20).

$$\begin{cases} a_n = \dfrac{2}{\pi}\displaystyle\int_0^{\pi} f(\omega t)\cos(n\omega t)d(\omega t) \\ b_n = \dfrac{2}{\pi}\displaystyle\int_0^{\pi} f(\omega t)\sin(n\omega t)d(\omega t) \end{cases} \tag{20}$$

And the plural form m_n of 2 coefficients a_n and b_n can also be expressed as

$$m_n = a_n + jb_n \tag{21}$$

Substitute the value of u_a in Fig.1 into (20).

$$\begin{cases} a_n = \dfrac{2}{n\pi}U_{dc}\displaystyle\sum_{k=1}^{N} g(\alpha_k)\sin n\alpha_k \\ b_n = -\dfrac{2}{n\pi}U_{dc}\displaystyle\sum_{k=1}^{N} g(\alpha_k)\cos n\alpha_k \end{cases} \tag{22}$$

The m_n can also be expressed as (23). The amplitude $|m_n|$ of the n_{th}-order harmonic can be obtained by finding the modulus of (23).

$$m_n = \frac{2U_{dc}}{jn\pi}\sum_{k=1}^{N} g(\alpha_k)e^{jn\alpha_k} \tag{23}$$

In addition, the a_n^2 and b_n^2 can be expressed as (24). Then the amplitude $|m_n|$ can be calculated as (25) in another method.

$$\begin{cases} a_n^2 = (\frac{2U_{\rm dc}}{n\pi})^2[\sum_{k=1}^{N}\sin^2 n\alpha_k + \sum_{\substack{i,j=1\\ i\neq j}}^{N} g(\alpha_i)g(\alpha_j) \\ \qquad \sin n\alpha_i \sin n\alpha_j] \\ b_n^2 = (\frac{2U_{\rm dc}}{n\pi})^2[\sum_{k=1}^{N}\cos^2 n\alpha_k + \sum_{\substack{li,j=1\\ i\neq j}}^{N} g(\alpha_i)g(\alpha_j) \\ \qquad \cos n\alpha_i \cos n\alpha_j] \end{cases} \tag{24}$$

$$|m_n| = \sqrt{a_n^2 + b_n^2} = \frac{2U_{\rm dc}}{n\pi}\sqrt{\sum_{i,j=1}^{N} g(\alpha_i)g(\alpha_j)\cos n(\alpha_i - \alpha_j)} \tag{25}$$

As shown in Fig.3, the change of switching angle is affected by the pulse edge state and current direction. The switching angles of $\alpha_k{}'$ with dead-time effects can be represented as (26).

$$\alpha_k{}' = \alpha_k + \frac{1 - {\rm sign}(i)g(\alpha_k)}{2}\omega_0 T_{\rm d} \tag{26}$$

Then Fourier coefficients with dead-time effects can be given as (27) for odd n, and the $n_{\rm th}$-order harmonic amplitude $|m_n{}'|$ with dead-time can be calculated from (28) or (29), as shown at the bottom of this page.

$$\begin{cases} a_n' = \dfrac{2U_{\rm dc}}{n\pi}\displaystyle\sum_{k=1}^{N} g(\alpha_k)\sin n[\alpha_k + \frac{1 - {\rm sign}(i)g(\alpha_k)}{2}\omega_0 T_{\rm d}] \\ b_n' = -\dfrac{2U_{\rm dc}}{n\pi}\displaystyle\sum_{k=1}^{N} g(\alpha_k)\cos n[\alpha_k + \frac{1 - {\rm sign}(i)g(\alpha_k)}{2}\omega_0 T_{\rm d}] \end{cases} \tag{27}$$

The $m_n{}'$ can also be expressed as

$$m_n' = \frac{2U_{dc}}{jn\pi}\sum_{k=1}^{N} g(\alpha_k)e^{jn\alpha_k'} \tag{28}$$

Defining $\theta_{ij} = [g(\alpha_i) - g(\alpha_i)]{\rm sign}(i)\omega_0 T_d/2$, angle θ_{ij} is subject to $\theta_{ij} = \omega_0 T_{\rm d}$ or $\theta_{ij} = -\omega_0 T_{\rm d}$ for the two adjacent i and j. Normally, $\theta_{ij} \neq 0$ if $T_{\rm d} \neq 0$. It is clear that $|m_n{}'| \neq |m_n|$ from comparing (25) with (29). Therefore, the dead-time effects change the harmonic characteristic of phase voltage $u_{\rm a}$. As the increase of dead-time $T_{\rm d}$, the content of harmonics will be increased due to the aggravated difference between $\alpha_i - \alpha_j + \theta_{ij}$ and $\alpha_i - \alpha_j$.

TABLE 1. The calculated amount of two methods.

	Method	$x\pm y$	$x/(\times)y$	e^x	$\sin(x)$
Without dead-time	Single	$4N$-1	$4N$+11	N	N
	Double	$3N$+2	$6N$+10	N+2	N
With dead-time	Single	$6N$-1	$5N$+13	N	N
	Double	$17N$-3	$24N$+16	$5N$+2	$2N$

C. COMPARISON BETWEEN DOUBLE FOURIER SERIES AND SINGLE FOURIER SERIES

In this subsection, the two harmonics analysis method are compared, and the link and difference between them are summarized.

A. The double Fourier series method is based on the respective angles of carrier wave and modulation wave to analyze their effects on harmonics, while the single Fourier series method is based on the same angle by converting the carrier angle into the angle of modulation wave.

B. The distribution of harmonics can be obtained by the formula based on double Fourier series method directly, as this method include both angles of carrier and modulation wave. In addition, double Fourier series method can also obtain the effect of the carrier ratio on harmonic distribution directly, as $\omega_0/\omega_{\rm c}$ is included in (9). However, the single Fourier series method can not get this information, as it only based on the angle of modulation wave.

C. The method based on single Fourier series can reduce computation largely. In this paper, the computation burden is evaluated from the following aspects: addition or subtraction, multiplication or division, exponential operation, and trigonometric operation. Table 1 shows the calculated amount of two methods. These calculations are represented as $x \pm y$, $x/(\times)y$, e^x, $\sin(x)$.

According to the comparison above, the applicable scenarios of the two methods can be summarized as follows: the double Fourier series method can be used, when it is necessary to analyze the specific regular of harmonic distribution or the relationship between harmonic distribution and carrier ratio. When the amplitude and content of each harmonic are the most important to be considered, the single Fourier series method can be used as it can reduce computation largely.

$$\begin{aligned} |m_n{}'| &= \frac{2U_{\rm dc}}{n\pi}\sqrt{\sum_{i,j=1}^{N-1} g(\alpha_i)g(\alpha_j)\cos n[\alpha_i - \alpha_j + \frac{g(\alpha_i) - g(\alpha_j)}{2}{\rm sign}(i)\omega_0 T_{\rm d}]} \\ &= \frac{2U_{\rm dc}}{n\pi}\sqrt{\sum_{i,j=1}^{N-1} g(\alpha_i)g(\alpha_j)\cos n[\alpha_i - \alpha_j + \theta_{ij}]} \end{aligned} \tag{29}$$

TABLE 2. System Parameters.

Parameters	Value
DC-link voltage U_{dc}/V	100
Fundamental frequency f_0/Hz	50
Carrier ratio N	125
Load resistance R/Ω	5
Load inductance L/mH	5

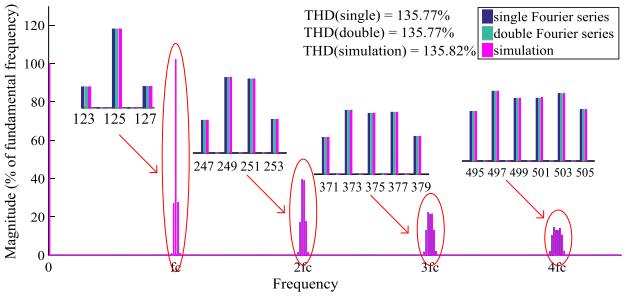

FIGURE 6. The harmonic spectrum of phase voltage without dead-time.

IV. SIMULATION AND EXPERIMENTAL RESULTS

In this section, simulation and experiment are performed to validate the effectiveness of the proposed theoretical analysis. The time-domain simulation is implemented in MATLAB/Simulink, and digital signal processor (DSP) TMS320F28335 is used as a controller in experiments. System parameters applied in simulation and experiment are listed in Table 2.

A. WITHOUT DEAD-TIME EFFECTS

Fig.6 shows the harmonic spectrums of phase voltage in theoretical calculation and simulation. The THDs of the phase voltage without dead-time calculated by simulation, the proposed single Fourier series, double Fourier series are 135.82%, 135.77%, 135.77%, respectively. During the theoretical calculation process, the initial phase is random setting for validating the proposed two calculation methods are more flexible than traditional method. It shows that the THDs calculated by different methods are almost the same. In addition, the each order harmonic contents which are calculated by simulation, single Fourier series and double Fourier series are the same. Therefore, the proposed harmonic quantitative calculation methods without dead-time are verified.

In Fig.6, according to the distribution of harmonic spectrum, the harmonic order near f_c are 123, 125, and 127. And the harmonic frequency around $2f_c$, $3f_c$, $4f_c$ can also be obtained from Fig.6. The regularity of spectrum distribution satisfies the analysis from (9), which obtains that the harmonic order $Nq+p$ is odd ($N = 125$ in this subsection). And it also satisfies the analysis in section IV that the harmonics of phase voltage contain only odd harmonics. Therefore, it proves the correctness of theoretical analysis.

B. WITH DEAD-TIME EFFECTS

In this paper, all experimental tests are set a dead-time due to security. The photo and parameters of experimental setup are shown in Fig.7 and Table 2, respectively. In this subsection,

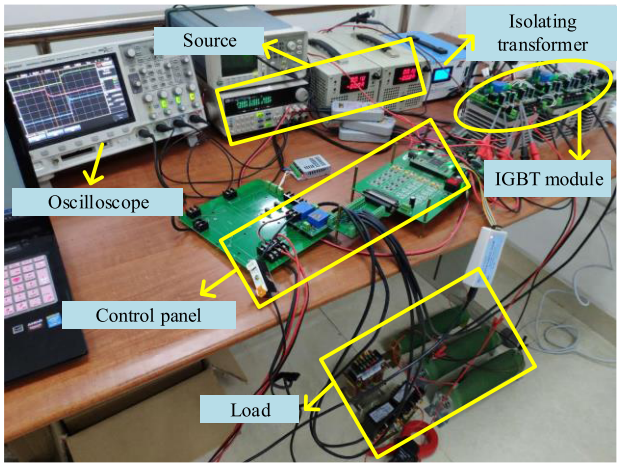

FIGURE 7. The photo of experimental setup.

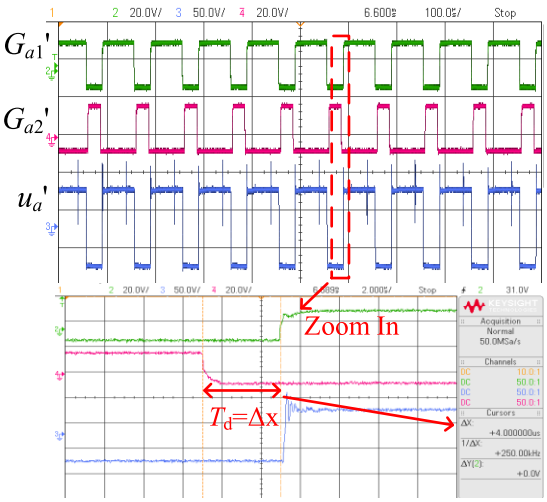

FIGURE 8. Drive signals for upper and lower arms.

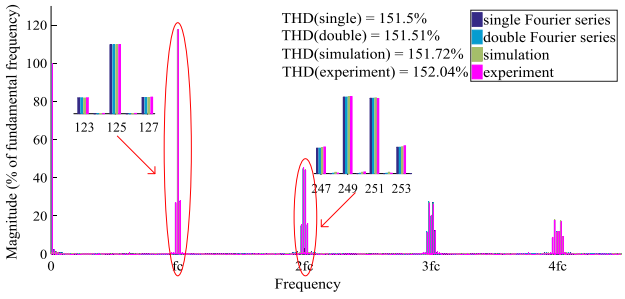

FIGURE 9. The harmonic spectrum of phase voltage with dead-time.

setting the parameter $T_d/T_c = 5/200$. Fig.8 shows the drive signals for upper and lower arms, and the phase voltage with dead-time. It can be seen that the wave in experiment is the same with the one analyzed in Fig.3. In addition, the dead-time T_d is 4μs as the carrier ratio $f_c/f_0 = 125$. Fig.9 shows the harmonic spectrum of phase voltage with dead-time effects. The THDs of the phase voltage with dead-time calculated by single Fourier series, double Fourier series,

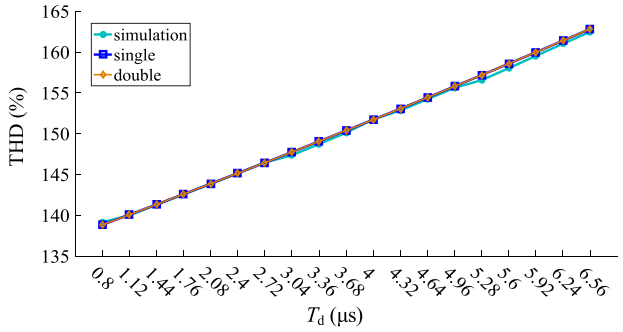

FIGURE 10. The THD of phase voltage with different dead-time T_d.

simulation, and experiment are 151.5%, 151.51%, 151.72%, and 152.04%, respectively, and the harmonic content obtained by different methods are almost the same. So the correctness of the proposed harmonic calculation methods of the phase voltage with dead-time is verified. In addition, the distributed regularity of the harmonic spectrum is the same as that without dead-time.

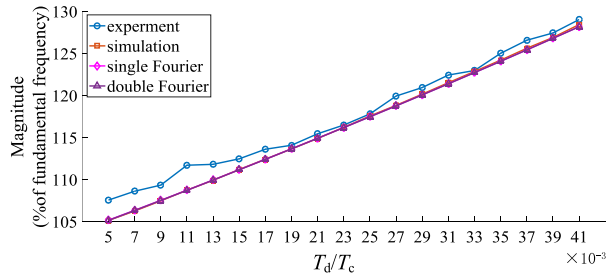

FIGURE 11. The highest harmonic magnitude in different T_d/T_c.

Fig.10 shows the THD of the phase voltage with different T_d and fixed T_c calculated by the proposed calculation methods and simulation. From Fig.10, the THD obtained by single Fourier series, double Fourier series and simulation is almost the same. Therefore, the two proposed harmonic calculation methods can be applicable to the operation conditions in different dead-time. Fig.11 shows the highest harmonic magnitude (harmonic order is 125) in different dead-time parameter T_d/T_c. The trends of the other harmonic are the same with the 125^{th}-order. It shows that the harmonic content is increasing as T_d/T_c increases. And the harmonic contents obtained by single Fourier series, double Fourier series, simulation, and experiment are almost the same. This also verifies the correctness of the proposed harmonic calculation methods of the phase voltage with dead-time. Fig.12 shows the harmonic spectrum of phase voltage in case of pure resistance. It can be seen that the harmonics obtained by the proposed calculation methods and simulation are almost the same. So the two proposed harmonic calculation methods are correct in condition of different output-loads.

Fig.13 shows the error between the highest harmonic magnitude obtained by experiment and the proposed theoretical calculation method without dead-time and with dead-time

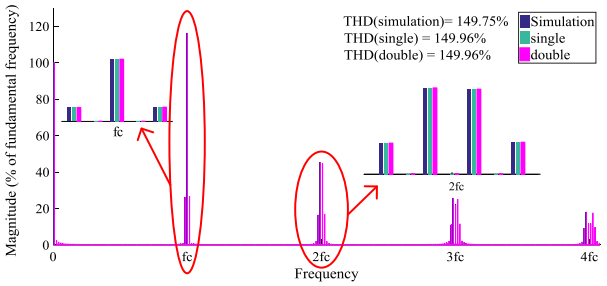

FIGURE 12. The harmonic spectrum in the case of pure resistance.

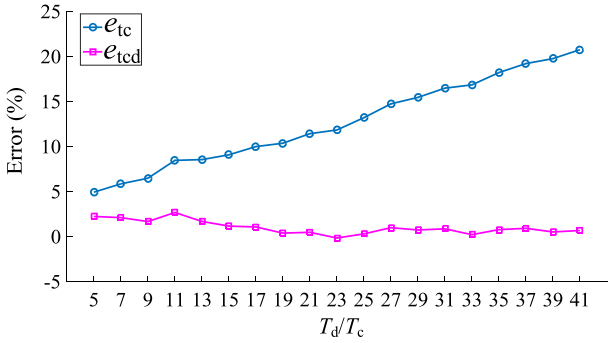

FIGURE 13. The harmonic errors in calculation without and with dead-time.

respectively. And the error is obtained by

$$\begin{cases} e_{tc} = \dfrac{M_{ex} - M_{tc}}{M_{ex}} \times 100\% \\ e_{tcd} = \dfrac{M_{ex} - M_{tcd}}{M_{ex}} \times 100\% \end{cases} \tag{30}$$

where M_{ex}, M_{tc} and M_{tcd} are the highest harmonic magnitude obtained by experiment and the proposed theoretical calculation method not considering dead-time effects and considering dead-time effects respectively; e_{tc} are defined as the error between M_{ex} and M_{tc}, e_{tcd} are defined as the error between M_{ex} and M_{tcd}.

It is obvious that the error increases when the effect of dead-time is not considered in theoretical calculation, but the error is almost zero while considering dead-time. Therefore, considering dead-time effects during calculating harmonics is necessary to accurately estimate the harmonic content especially when T_d/T_c is not small.

C. COMPARATIVE ANALYSIS

Take the condition that $f_c/f_0 = 125$, $T_d/T_c = 0.025$ for example, the highest harmonic content around f_c obtained by experiment, simulation, the proposed single Fourier series with and without dead-time, and double Fourier series with and without dead-time are listed in TABLE 3. In addition, the calculated quantities of the theoretical methods are also shown in TABLE 3. Based on this comparison table, the magnitude of harmonics obtained by single- and double- Fourier series with dead-time are almost the same that in experiment and simulation, while the errors of the harmonic magnitude

TABLE 3. Comparative analysis.

Method		Harmonic content (f_c)	Calculated Quantities			
		125th-order	$x\pm y$	$x/(\times)y$	e^x	$\sin(x)$
experiment		117.8				
simulation		117.6				
single	without	102.3	499	511	125	125
	with	117.5	749	638	125	125
double	without	102.3	377	760	127	125
	with	117.5	2122	3016	627	250

obtained by the two theoretical methods without dead-time are relatively large. Therefore, the calculation results of harmonics will be more accurate when considering the dead-time effects.

Based on Table 1, the calculated amounts of the two theoretical methods with or without dead-time are listed in Table 3. It is obvious that the proposed single Fourier series method has smaller computational resources and will have a faster computing speed than the double Fourier series under the same calculation accuracy and computing platform. The calculated amounts of the double Fourier method for each algorithm are more than two times as much as that of the single Fourier method, when considering dead-time.

V. CONCLUSION

This paper presents two harmonic quantitative analysis methods for dead-time effects in PWM converters. The closed form solution of phase voltage harmonics in SPWM converter with and without dead-time based on double- and single- Fourier series are deduced. Both the two proposed calculated methods can be applicable in any initial phase case. The inner link and different between the two proposed harmonics analysis methods and the harmonic mechanism caused by dead-time effects are revealed. The the applicable scenarios of the two methods are summarized respectively. A novel method to calculate the switching angles of regular sampling SPWM is presented. Comparative analysis by theory calculations, simulation and experiment results shows that the closed form solutions of harmonics in the proposed methods are correct, and the proposed single Fourier series method is more concise. In addition, the analysis from the proposed harmonic calculation expression and experiment results show the duration of dead-time have significant effects on harmonic characteristics, where the harmonics will be aggravated as the increase of dead-time. It is necessary to consider dead-time effects in harmonic calculation when T_d/T_c is not small and such calculation result are much more accurate.

REFERENCES

[1] R. R. Chilipi, N. Al Sayari, A. R. Beig, and K. Al Hosani, "A multitasking control algorithm for grid-connected inverters in distributed generation applications using adaptive noise cancellation filters," *IEEE Trans. Energy Convers.*, vol. 31, no. 2, pp. 714–727, Jun. 2016.

[2] N. Saadat, S. S. Choi, and D. M. Vilathgamuwa, "A series-connected photovoltaic distributed generator capable of enhancing power quality," *IEEE Trans. Energy Convers.*, vol. 28, no. 4, pp. 1026–1035, Dec. 2013.

[3] A. M. Marzouki Hamouda and F. Fnaiech, "A review of PWM voltage source converters based industrial applications," in *Proc. ESARS*, Aachen, Germany, Mar. 2015, pp. 1–6.

[4] M. Kumar and R. Gupta, "Time-domain characterisation of multicarrier-based digital SPWM of multilevel VSI," *IET Power Electron.*, vol. 11, no. 1, pp. 100–109, Jan. 2018.

[5] Y. Zhao, W. Qiao, and L. Wu, "Dead-time effect analysis and compensation for a sliding-mode position observer-based sensorless IPMSM control system," *IEEE Trans. Ind. Appl.*, vol. 51, no. 3, pp. 2528–2535, May 2015.

[6] Y. Qi, J. Fang, J. Liu, and Y. Tang, "Coordinated control for harmonic mitigation of parallel voltage-source inverters," *CES Trans. Elect. Mach. Syst.*, vol. 2, no. 3, pp. 276–283, Sep. 2018.

[7] H. Hu, Z. He, X. Li, K. Wang, and S. Gao, "Power-quality impact assessment for high-speed railway associated with high-speed trains using train timetable—Part I: Methodology and modeling," *IEEE Trans. Power Del.*, vol. 31, no. 2, pp. 693–703, Apr. 2016.

[8] Q. N. Trinh, P. Wang, Y. Tang, and F. H. Choo, "Mitigation of DC and harmonic currents generated by voltage measurement errors and grid voltage distortions in transformerless grid-connected inverters," *IEEE Trans. Energy Convers.*, vol. 33, no. 2, pp. 801–813, Jun. 2018.

[9] U.-M. Choi, J.-S. Lee, and K.-B. Lee, "New modulation strategy to balance the neutral-point voltage for three-level neutral-clamped inverter systems," *IEEE Trans. Energy Convers.*, vol. 29, no. 1, pp. 91–100, Mar. 2014.

[10] Y. Wang, X. Wang, F. Blaabjerg, and Z. Chen, "Harmonic instability assessment using state-space modeling and participation analysis in inverter-fed power systems," *IEEE Trans. Ind. Electron.*, vol. 64, no. 1, pp. 806–816, Jan. 2017.

[11] D. Arricibita, P. Sanchis, R. Gonzalez, and L. Marroyo, "Impedance emulation for voltage harmonic compensation in PWM stand-alone inverters," *IEEE Trans. Energy Convers.*, vol. 32, no. 4, pp. 1335–1344, Dec. 2017.

[12] H. Cui, W. Song, H. Fang, X. Ge, and X. Feng, "Resonant harmonic elimination pulse width modulation-based high-frequency resonance suppression of high-speed railways," *IET Power Electron.*, vol. 8, no. 5, pp. 735–742, Apr. 2015.

[13] S. R. Bowes and B. M. Bird, "Novel approach to the analysis and synthesis of modulation processes in power convertors," *Proc. Inst. Elect. Eng*, vol. 122, pp. 507–513, May 1975.

[14] J. Shen, J. A. Taufiq, and A. D. Mansell, "Analytical solution to harmonic characteristics of traction PWM converters," *IEE Proc.-Electr. Power Appl.*, vol. 144, no. 2, pp. 158–168, Mar. 1997.

[15] H. Deng, L. Helle, Y. Bo, and K. B. Larsen, "A general solution for theoretical harmonic components of carrier based PWM schemes," in *Proc. APEC*, Feb. 2009, pp. 1698–1703.

[16] M. Odavic, M. Sumner, P. Zanchetta, and J. C. Clare, "A theoretical analysis of the harmonic content of PWM waveforms for multiple-frequency modulators," *IEEE Trans. Power Electron.*, vol. 25, no. 1, pp. 131–141, Jan. 2010.

[17] I. Dolguntseva, R. Krishna, D. E. Soman, and M. Leijon, "Contour-Based dead-time harmonic analysis in a three-level neutral-point-clamped inverter," *IEEE Trans. Ind. Electron*, vol. 62, no. 1, pp. 203–210, Jan. 2015.

[18] C. M. Wu, W.-H. Lau, and H. S.-H. Chung, "Analytical technique for calculating the output harmonics of an H-bridge inverter with dead time," *IEEE Trans. Circuits Syst. I, Fundam. Theory Appl.*, vol. 46, no. 5, pp. 617–627, May 1999.

[19] M. Kumar, "Time-domain characterization of digitized PWM inverter with dead-time effect," *IEEE Trans. Circuits Syst. I, Reg. Papers*, vol. 65, no. 10, pp. 3592–3601, Oct. 2018.

[20] G. Fedele and D. Frascino, "Spectral analysis of a class of DC–AC PWM inverters by Kapteyn series," *IEEE Trans. Power Electron.*, vol. 25, no. 4, pp. 839–849, Apr. 2010.

[21] D. J. Kostic, Z. Z. Avramovic, and N. T. Ciric, "A new approach to theoretical analysis of harmonic content of PWM waveforms of single- and multiple-frequency modulators," *IEEE Trans. Power Electron.*, vol. 28, no. 10, pp. 4557–4567, Oct. 2013.

[22] H. D. T. Mouton, B. McGrath, D. G. Holmes, and R. H. Wilkinson, "One-dimensional spectral analysis of complex PWM waveforms using superposition," *IEEE Trans. Power Electron.*, vol. 29, no. 12, pp. 6762–6778, Dec. 2014.

[23] B. McGrath and H. D. T. Mouton, "One-dimensional spectral analysis techniques for multilevel PWM strategies," *IEEE Trans. Power Electron.*, vol. 31, no. 10, pp. 6910–6919, Oct. 2016.

[24] D. G. Holmes and T. A. Lipo, "Modulation of one inverter phase leg," in *Pulse Width Modulation for Power Converters: Principles and Practice*. Hoboken, NJ, USA: Wiley, 2003, pp. 257–295.

NING JIAO was born in Hebei, China, in 1994. She received the B.S. degree from Sichuan University, Chengdu, China, in 2018, where she is currently pursuing the master's degree with the College of Electrical Engineering and Information Technology.

Her current research interests include modulation of power converters and high voltage direct current.

SHUNLIANG WANG (M'18) received the B.S. and Ph.D. degrees in electrical engineering from Southwest Jiaotong University, Chengdu, China, in 2010 and 2016, respectively.

From 2017 to 2018, he was a Visiting Scholar with the Department of Energy Technology, Aalborg University, Denmark. He is currently an Associate Research Fellow with the College of Electrical Engineering and Information Technology, Sichuan University. His current research interests include digital control and modulation of power converters in railway traction systems, and high voltage direct current.

TIANQI LIU (SM'16) received the B.S. and M.S. degrees from Sichuan University, Chengdu, China, in 1982 and 1986, respectively, and the Ph.D. degree from Chongqing University, Chongqing, China, in 1996, all in electrical engineering. She is currently a Professor with the College of Electrical Engineering and Information Technology, Sichuan University. Her research interests include power system analysis and stability control, HVDC, optimal operation, dynamic security analysis, dynamic state estimation, and load forecast.

YANBO WANG (S'15–M'17) received the Ph.D. degree from the Department of Energy Technology, Aalborg University, Denmark, in 2017, where he is currently with the Department of Energy Technology, as a Postdoctoral Fellow. In 2016, he was a Visiting Scholar with the Power System Research Group, Department of Electrical and Computer Engineering, University of Manitoba, Winnipeg, MB, Canada. His research interests include distributed power generation systems, wind power systems, microgrid, as well as operation and control technologies of power electronic-dominated power systems. His paper on Distributed Power System received the First Prize Paper Award of the 6th International Conference of Smart Grid cosponsored by the IEEE Industry Application Society, in 2017. He received the Best Session Paper Award at the annual conference of the IEEE Industrial Electronics Society, in 2015, in Japan.

ZHE CHEN (M'95–SM'98–F'18) received the B.Eng. and M.Sc. degrees from the Northeast China Institute of Electric Power Engineering, Jilin, China, and the Ph.D. degree from the University of Durham, U.K.

He is currently a Full Professor with the Department of Energy Technology, Aalborg University, Denmark. He is also the Leader of the Wind Power System Research Program, Department of Energy Technology, Aalborg University, and the Danish Principle Investigator for Wind Energy of Sino-Danish Centre for Education and Research. He has led many research projects and has more than 500 publications in his technical field. His research interests include power systems, power electronics and electric machines, and his main current research interests include wind energy and modern power systems.